Catalysis Today 449 (2025) 115204

Contents lists available at ScienceDirect

Catalysis Today

journal homepage: www.elsevier.com/locate/cattod

Effect of Ce:Ti ratio and cerium salts on the properties of mesoporous Ti-Ce oxides and their photocatalytic activity

Peter Nadrah [a], Mateja Knap [a,b], Tatiparthi Vikram Sagar [b], Andrijana Sever Škapin [a,c], Urška Lavrenčič Štangar [b,*]

[a] Slovenian National Building and Civil Engineering Institute, Dimičeva ulica 12, Ljubljana 1000, Slovenia
[b] University of Ljubljana, Faculty of Chemistry and Chemical Technology, Večna pot 113, Ljubljana 1000, Slovenia
[c] Faculty of Polymer Technology, Ozare 19, Slovenj Gradec 2380, Slovenia

ARTICLE INFO

Keywords:
Ti-Ce oxides
Evaporation-induced self-assembly
Isopropanol oxidation
Photocatalysis
Mesoporous material

ABSTRACT

To investigate the influence of different CeO_2 precursors and Ce:Ti ratios, we have synthesised 8 mesoporous Ti-Ce oxides via the evaporation-induced self-assembly (EISA) method with Ce:Ti ratios between 0.2 and 20 mol%. The materials exhibited type IV isotherms and a specific surface area of 140–180 $m^2 \cdot g^{-1}$ with pore diameters in range of 3–20 nm. The crystalline phases of materials comprised predominantly anatase with a significant decrease in overall crystalline content with increasing Ce:Ti ratio. Materials with higher Ce:Ti ratio showed an increased light absorption in the visible region. Although crystalline CeO_2 was not detected, the presence of Ce (IV) was confirmed by X-ray photoelectron spectroscopy. For the photocatalytic experiments, we compared these materials with the TiO_2-CeO_2 composites of our previously published syntheses to yield 16 samples synthesized via three synthesis approaches: (1) concurrent synthesis from titanium alkoxide and cerium salts in one pot, (2) synthesis of TiO_2 in the presence of previously-synthesised CeO_2 and (3) physical mixing of separately-synthesised TiO_2 and CeO_2. Samples produced by physically mixing the separately-synthesised TiO_2 and CeO_2 showed the best photocatalytic activity towards gaseous isopropanol degradation, while the samples with TiO_2 synthesised in the presence of CeO_2 showed the best photocatalytic stability.

1. Introduction

Photocatalysis is the process of using light to catalyse chemical reactions. While much attention is given to the use of photocatalysts to produce energy-rich compounds, namely by reduction of CO_2 to energy-rich hydrocarbons and water splitting to hydrogen and oxygen[1] under solar irradiation, other photocatalytically-driven reactions are also important from the environmental and sustainability viewpoint; namely, degradation of pollutants[2] and conversion of organic compounds into other value-added compounds[3]. TiO_2 alone is a powerful photocatalyst under certain conditions, but possesses unfavourable properties, such as high recombination rate of photogenerated electrons and oxygen vacancies and negligible absorption of visible component of the solar irradiation[4]. Introduction of other photocatalysts[5], co-catalysts[1,6] and dopants improves its photocatalytic activity. TiO_2-CeO_2 composite materials are one of such materials, which showed increased visible light absorption and photocatalytic activity compared to pure TiO_2[7]. CeO_2 is another photocatalyst with high stability, low toxicity[8] and the ability of cerium to shift between the Ce^{3+} and Ce^{4+} states[9].

Mesoporous materials are defined as porous materials with 2–50 nm pore size according to IUPAC. Their large specific surface area offers a large area where photocatalytic reactions can occur. One of the most common methods to synthesise mesoporous oxides is a sol-gel method using soft templating method. In contrast to the classical sol-gel synthesis, in the evaporation-induced self-assembly (EISA) method[10] of synthesis, the reactor temperature and relative humidity are controlled to slowly evaporate the volatile compounds, induce micelle formation of the template molecules (surfactants) and form a gel-like product. During the reaction, the metal precursors hydrolyse and condense to inorganic oxides around these micelles to yield a mesoporous structure[11–13]. EISA is a good choice for preparation of metal oxides from highly reactive alkoxides, such as titanium alkoxides, as was recently demonstrated by the synthesis of mesoporous TiO_2 with a well-ordered hexagonal (*P6mm*) pore arrangement[14].

TiO_2-CeO_2 composites were synthesized and tested for degradation

* Corresponding author.
E-mail address: urska.lavrencic.stangar@fkkt.uni-lj.si (U. Lavrenčič Štangar).

https://doi.org/10.1016/j.cattod.2025.115204
Received 30 September 2024; Received in revised form 17 December 2024; Accepted 12 January 2025
Available online 16 January 2025

of methylene blue and 4-chlorophenol[15]; TiO_2-CeO_2 and TiO_2-CeO_2-ZrO_2 were investigated for Rhodamine B photocatalytic degradation[16]; ball-milled TiO_2-CeO_2-CuO for CO_2 photoreduction to ethanol [17]; TiO_2-CeO_2 composites for phenol[7] and 4-chlorophenol[18] degradation, methanol steam reforming[19]; and Ce-doped TiO_2 for Rhodamine B degradation[20]. Different sources of CeO_2 are used during the sol-gel synthesis of TiO_2-CeO_2 composites: cerium nitrate is the most widely used[21–27], other CeO_2 precursors, such as cerium ammonium nitrate[28], cerium acetate[29] and cerium alkoxides[30] are less common. It is also possible to use previously-synthesised CeO_2, either added to the sol-gel synthesis of TiO_2 from titanium alkoxides [31–33] or physically mixed with previously-synthesised TiO_2[34,35]. We investigated both approaches recently[36]. Zaharescu et al.[29] compared TiO_2-CeO_2 synthesized via sol-gel method with different CeO_2:TiO_2 ratios and two CeO_2 precursors: cerium nitrate and cerium acetate. When cerium nitrate (soluble in the reaction mixture) was used, they observed incorporation of cerium ions in TiO_2 at lower CeO_2:TiO_2 ratios and unreacted cerium precursor still present at higher CeO_2:TiO_2 ratios. On the other hand, cerium acetate (only partially soluble in the reaction mixture) reacted to form CeO_2 only after precipitation of the titanium precursor. They used moderate ratios of CeO_2:TiO_2, namely 20:80 and 50:50. To the best of our knowledge there have been no reports on the influence of precursors and Ce:Ti ratio on the synthesis of mesoporous Ti-Ce oxides using EISA method. If we understood the influence of precursors and Ce:Ti ratio, we could design materials better suited for the intended application.

We have previously reported on TiO_2-CeO_2 composites synthesized via EISA and their use in photocatalytic CO_2 reduction and H_2 production[36]. In that report, we synthesized CeO_2 separately and then used two approaches to form the composites: (i) synthesis of TiO_2 in the presence of CeO_2 and (ii) physical mixing of separately-synthesized TiO_2 and CeO_2.

Herein, we report on the mesoporous Ti-Ce oxides synthesized concurrently from titanium alkoxide and two cerium salts with Ce:Ti molar ratios from 0 to 20 mol%. We compare the chemical properties and photocatalytic activity of isopropanol oxidation of these materials with the TiO_2-CeO_2 composites prepared by the two approaches stated above with the same Ce:Ti molar ratios.

2. Experimental

The following chemicals were used in the experiments: titanium butoxide (TBOT) (Merck Sigma-Aldrich), cerium acetate (Aldrich), cerium nitrate hexahydrate (Aldrich), Pluronic F127 (Sigma), 36 % hydrochloric acid (Merck Supelco), acetic acid (Honeywell Fluka), HPLC grade water (Honeywell Riedel-de Haën), isopropanol (Honeywell Riedel-de Haën), ethanol (Honeywell Riedel-de Haën) and butan-1-ol (Sigma-Aldrich).

2.1. Ti-Ce oxide synthesis

Ti-Ce oxides were synthesized using EISA method with four different amounts of cerium species (0.2, 1, 5 and 20 mol% as molar Ce:Ti ratio). Pure TiO_2 was synthesized separately following the same procedure but without the cerium source. The synthesis consisted of three main steps. Two cerium salts (cerium(III) acetate or cerium(III) nitrate hexahydrate) were used as cerium sources. The cerium salt was dissolved in ethanol (34 mL), followed by addition of 36 % hydrochloric acid (2.5 mL), acetic acid (1.68 mL), water (up to the total amount of 10 equiv.) and Pluronic F127 (1.85 g) in a 100 mL round bottom flask and then stirred and heated at 40 °C for 1 hour. Afterwards, titanium(IV) butoxide (5 mL, 1 equiv.) was slowly added to the solution and stirred for an additional hour at 40 °C. The reaction mixture was then transferred to petri dishes and placed in a chamber with a temperature of 40 °C and relative humidity (RH) of 33 % for 24 hours to evaporate the volatile compounds. Afterwards, the obtained gel was calcined for 4 hours at 400 °C with a heating ramp 1 $K{\cdot}min^{-1}$. Finally, the material was crushed for 10 minutes in an agate mortar.

2.2. Characterization

The Ti-Ce oxides were characterized with scanning electron microscopy (SEM), X-ray powder diffraction, nitrogen sorption, X-ray photoelectron spectroscopy (XPS), inductively coupled plasma optical emission spectroscopy (ICP-OES) and photoluminescence spectroscopy (PL). The details of the used methods are described in the Supplementary Materials.

2.2.1. Determination of photocatalytic activity

Appropriate mass of butan-1-ol was added to around 50 mg of a sample to prepare a 12 wt% suspension. The suspension was vigorously shaken and a portion of it (0.33–0.35 g) was evenly spread on the round glass holder (diameter 60 mm). After 2 hours of drying, a thin film of material was obtained. Sample was stored overnight in the dark at 33 % RH. The equipment for determination of photocatalytic activity in gas-solid system (Figure S6) consisted of a reactor system with a capacitive humidity and temperature sensor, UV-Vis Xe lamp (Newport) and Fourier-transform infrared spectroscopy (FTIR) spectrometer (Perkin Elmer Spectrum Two) with gas FTIR cell. Photocatalytic activity of samples was determined by oxidation of isopropanol (model pollutant) to acetone. Sample was placed in a reactor, hermetically sealed with a quartz glass, and covered to protect from light. The air in the reactor was dried and then humidified to 33 % RH. 8 μL of isopropanol were injected into the reactor, yielding approx. 800 ppm in the reactor. After 1 hour, the sample was irradiated with the UV-Vis Xe lamp (irradiance: approx. 20 $W{\cdot}m^{-2}$ in the range 300–400 nm) for 30 minutes. The decreasing concentration of isopropanol and increasing concentration of acetone were monitored using the FTIR spectrometer with the gas cell. The activity of the catalyst was calculated from the slope of the rising acetone concentration from 80 spectra collected in the first 6 minutes of irradiation and given in $ppm{\cdot}h^{-1}$. The method provides a good linear fit ($R^2 > 0.99$) in the specified time interval.

2.2.2. Determination of photocatalytic stability

The procedure for measuring the photocatalytic activity was repeated three times. After each measurement, the sample was placed in the fume hood to desorb any adsorbed compounds during the measurement and then placed in a chamber with 33 % RH up until the next measurement, constituting one cycle.

3. Results and discussion

We synthesized mesoporous Ti-Ce oxides using EISA method using two cerium precursors: cerium acetate and cerium nitrate labelled TCA-X and TCN-X, respectively, where X denotes percentile of Ce:Ti molar ratio (mol%) – 0.2, 1, 5 and 20 (1 mol% equals Ce:Ti ratio of 1:100). Pure TiO_2 (label T-0) was synthesized separately following the same method but without the cerium salt.

We confirmed the Ce:Ti ratio using ICP-OES method. The obtained values match well the theoretical values with most of the samples within 16 % relative deviation between the two values (Table 1).

Scanning electron microscopy (SEM) of the selected Ti-Ce oxides showed agglomerates without clear boundaries as presented in Figure S1. After the EISA synthesis, the products were in the form of a self-standing film (1–2 mm thick), thus a product in the form of an interconnected network is expected.

The phase structure of Ti-Ce oxides was determined with XRD analysis. The diffractograms presented in Fig. 1 exhibit reflections at 25.5°, 37.9°, 48.0°, 54.5°, 62.8° and 75.0°, which can be attributed to anatase TiO_2 (ICDD No. 21–1272) and reflections at 27.7°, 36.1° and 41.3°, which can be attributed to rutile TiO_2 (ICDD No. 21–1276). Crystalline phases for TCA and TCN samples comprised predominantly

Table 1
List of synthesised materials with theoretical Ce:Ti ratio and ratio determined with ICP-OES. [a] Relative deviation calculated using $\frac{meas.\,(Ce:Ti) - theor.\,(Ce:Ti)}{theor.\,(Ce:Ti)}$.

Sample name	Theoretical Ce:Ti	Measured Ce:Ti	Relative deviation[a]
	[mol%]	[mol%]	[%]
T-0	0.0	0.00	0
TCA-0.2	0.2	0.17	−16
TCA-1	1.0	0.90	−10
TCA-5	5.0	5.78	16
TCA-20	20.0	22.37	12
TCN-0.2	0.2	0.19	−6
TCN-1	1.0	0.96	−4
TCN-5	5.0	5.97	19
TCN-20	20.0	23.14	16

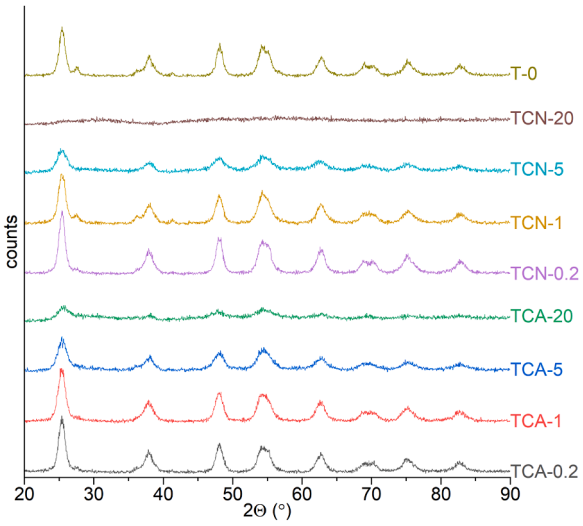

Fig. 1. Diffractograms of the samples TCA, TCN and pure TiO_2 (T-0) as a reference (curves are offset on the y-axis).

anatase and a small amount of rutile (up to 13 %); the exact numbers are given in the supplementary information (Table S1). The XRD analysis did not reveal crystalline CeO_2 in any samples. The diffractograms presented in Fig. 1 show considerable peak broadening and decrease in intensity for higher Ce:Ti ratios, which suggest high amount of amorphous phases. This is especially evident in samples with the highest Ce:Ti ratio (TCA-20 and TCN-20), which exhibit too broad peaks for reliable identification of crystalline phases. Of these two, TCA-20 exhibits broad peaks that could be identified as a reflection of anatase, but the presence of crystalline cerium species could not be detected. These results are similar to those obtained by Zaharescu[29], who obtained predominantly amorphous powder after sol-gel synthesis of TiO_2-CeO_2 (TiO_2:CeO_2 ratio 80:20) from titanium isopropoxide and cerium nitrate. However, when they used cerium acetate as CeO_2 source, they obtained sufficiently crystallized material for the determination of the phases (anatase and cerianite). Due to the significant mismatch between the sizes of Ce^{3+}/Ce^{4+} (0.103 nm/0.102 nm) and Ti^{4+} (0.068 nm) it is not expected for Ce^{3+} or Ce^{4+} cations to be able to replace Ti^{4+} cations in the lattice of TiO_2[37–39]. Thus, it is more likely that cerium species are dispersed on the surface of TiO_2 and can form Ti-O-Ce bonds[26]. The absence of CeO_2 reflections in similar syntheses with n(Ce:Ti) = 0.05 was noticed before[15]. They concluded that CeO_2 species were highly dispersed in the TiO_2 network. Similarly, Xiao et al.[20] reported on diffraction peaks broadening for Ce-doped TiO_2 via hydrothermal synthesis.

Nitrogen sorption analysis was performed to investigate the mesoporous structure. The isotherms (Fig. 2A) exhibit type IV according to IUPAC with a hysteresis loop of types H1 and H2. Thermal treatment is often expected to partially collapse the mesoporous structure above a certain temperature or duration (depending on the material). Here, TCA-20 exhibits H1 hysteresis loop in a relatively narrow p/p_0 range with steep isotherm slopes in that region, which can indicate well-ordered mesoporous structure. Other TCA and TCN samples exhibit hysteresis loop spanning a larger range of p/p_0 with less steep slopes. Pore width distributions (Fig. 2B) show predominantly pores in the 3–20 nm range. Pore size distribution peaks are located at 17 nm and 9 nm for TCA-20 and TCN-20, respectively, while the peaks are in the 7–8 nm range for other samples.

The pore volumes range from 0.30 to approx. 0.45 $cm^3 \cdot g^{-1}$ (Fig. 2C). In general, an increase of pore volume is observed for TCA samples with an increase of Ce:Ti ratio. In contrast, a decrease is observed for TCN from 1 to 5 mol%. BET specific surface area (S_{BET}) values given in Fig. 2C show values for S_{BET} of the materials in the range 140–180 $m^2 \cdot g^{-1}$. These two sample groups show an increase of S_{BET} with increasing Ce:Ti ratio up to 5 mol% and then a decrease for 20 mol%. Xiao et al.[20] ascribed increased S_{BET} of Ce-doped TiO_2 to prevention of mesopores collapse and anatase-to-rutile phase transition. Pure CeO_2 synthesised using the same method has much lower S_{BET} (14 $m^2 \cdot g^{-1}$) [36]. This effect, however, cannot produce even higher S_{BET} at the highest Ce:Ti ratios (20 mol%), where the effect of lower TiO_2 content, responsible for the mesoporous structure, dominates. The crystallite sizes of anatase were calculated using Scherrer equation. The plot in Fig. 2D shows strong decrease with increasing Ce:Ti ratio. In these samples, the addition of cerium salts evidently inhibits the growth of anatase crystallites as well as the transition from amorphous to crystalline phase as shown above. Smaller crystallite sizes with increasing Ce:Ti ratio coincide well with the increase of S_{BET}.

The surface of the samples was analysed using XPS. Ce 3d XPS spectra of TCA-20 and TCN-20 has been deconvoluted into eight peaks attributed to the spin-orbit splitting of different 3d levels and presented in the Figs. 3B and 3D (spectra of other samples are provided in Figure S2). These peaks illustrate the co-existence of Ce^{3+} and Ce^{4+} in the solids[40,41]. The binding energies (BE) at 881.3, 882.9, 885.3, 898.9 eV and the peaks at 900.9, 903.9, 908.1, 916.7 eV represent the Ce $3d_{5/2}$ and Ce $3d_{3/2}$, respectively. Similar peaks are observed in TCA-20 and TCN-20 representing that both precursors lead to similar interactions with the adjacent metal Ti. The surface concentration of Ce^{3+} is calculated according to the previous literature[42], u''' at 916.7 eV representing the Ce^{4+} peak does not overlap with any other peaks, so it is convenient one to use to measure the ratio $c(Ce^{4+}) / (c(Ce^{3+}) + c(Ce^{4+}))$. The ratio is calculated by using the integral area of u''' (A_u''') divided by the total area of Ce 3d ($A_{Ce\ 3d}$). Here, the values of $A_u'''/A_{Ce\ 3d}$ are 0.06744 and 0.05999 for TCA-20 and TCN-20, respectively, meaning 6–7 % surface Ce is present in oxidation state + 4. At lower Ce:Ti ratios the majority of cerium is present in Ce^{3+} form. This indicates only partial transformation of cerium salt to CeO_2 at high Ce:Ti ratios and presumably no transformation to CeO_2 at lower Ce:Ti ratios. The same synthesis method without TiO_2 precursors, however, yielded crystalline CeO_2. Ti 2p XPS spectra of TCA-20 and TCN-20 are presented in the Figs. 3A and 3C (spectra of other samples are provided in Figure S3). The peaks at 458.2 and 464.0 eV are attributed to Ti $2p_{3/2}$ and Ti $2p_{1/2}$, respectively. According to the literature[43], the pure TiO_2 (i.e., Ti^{4+}) shows a peak at 459.4 eV, and the Ce addition leads to shifting the BE value to 457.9 eV. This phenomenon indicates generation of an intermediate oxidation state of Ti, i.e., the presence of Ti^{3+} in the material. In accordance with the above study, Ce addition leads to a decrease in the Ti $2p_{3/2}$ peak to a value of 458.2 eV, representing the presence of a lower oxidation state of Ti (Ti^{3+}). This phenomenon is observed in both, TCA-20 and TCN-20. It was shown[43] that the addition of Ce produces a noticeable shift from 534 to 529 eV in O 1 s XPS spectra, indicating that both metal interactions with the oxygen increase with an increase of Ce content. Here, the same O 1 s peak

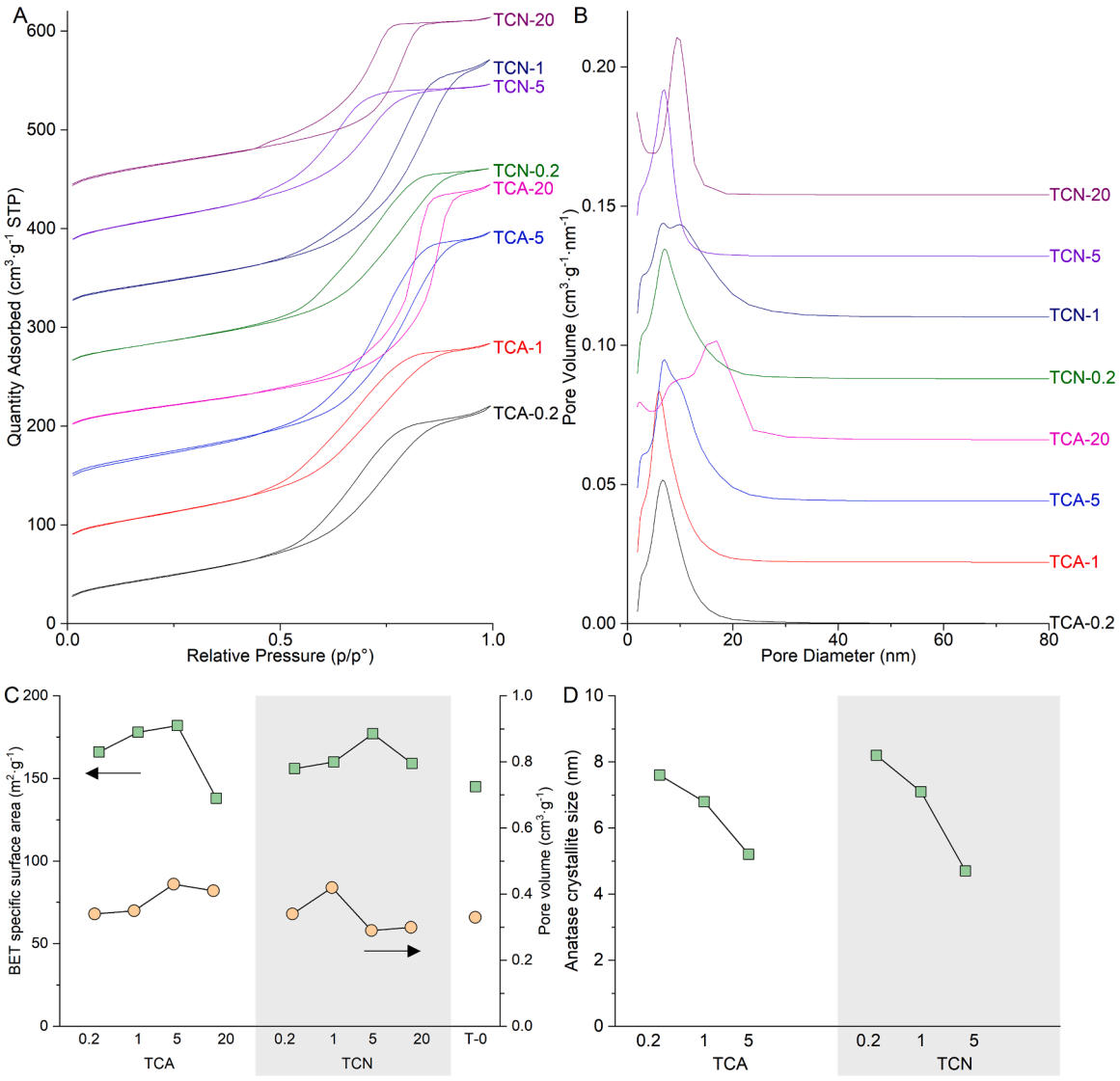

Fig. 2. (A) Nitrogen sorption isotherms (curves are offset by 60 $cm^3 \cdot g^{-1}$) and (B) distribution of pore diameters (curves are offset by 0.022 $cm^3 \cdot g^{-1} \cdot nm^{-1}$) for Ti-Ce oxides. (C) Specific surface area determined by BET (left axis) and pore volume (right axis) of the synthesized materials and (D) crystallite size for anatase calculated with Scherrer equation from diffractograms.

(Figure S4) showing at BE 529 eV corresponds to the lattice O of Ti-Ce oxides indicating high interactions of both metal oxides and possible formation of Ti-O-Ce bonds. The two large humps in spectra presented in Figure S4 for samples TCA-0.2, TCA-5 and TCA-20 can be deconvoluted into two peaks at 531.9 and 533.5 eV, which can be attributed to the loosely-bound adsorbed oxygen or water adsorbed on the vacant lattice sites[42]. In the TCN materials, these peaks appear with low intensity, indicating that the loosely-bound adsorbed oxygen is negligible compared to the TCA materials.

We analysed the spectroscopic characteristics of the materials also using diffuse reflectance spectroscopy (DRS). TCA and TCN samples with the lowest Ce content have spectra similar to the pure TiO_2[36] as depicted in Fig. 4A and C. Higher Ce:Ti ratios, particularly 20 mol%, exhibit a decrease at 510 nm and below. Lower absorption in 350–400 nm region was also reported for amorphous TiO_2 compared to rutile[44] and anatase[45]. Lower reflectance in 400–500 nm range can be attributed to the formation of amorphous CeO_2 or Ti-O-Ce bonds. Since a similar trend is observed in the case of cerium nitrate (TCN) and cerium acetate (TCA) and since the acetic acid is also present as a reactant, we postulate that the main effect is caused by the presence of Ce^{3+}/Ce^{4+} ions, not the anion of the reactant. Liu et al.[46] reported a similar increase of absorption in the 400–500 nm range for Ce-doped TiO_2. The Tauc plots presented in Fig. 4B and D were constructed to calculate the band gaps. These values were derived from the intercept of the linear fit to the linear slope of the curve with the x-axis. The values show a decrease with increasing Ce:Ti ratio: 3.00, 2.81, 2.33 and 2.17 eV for TCA-0.2 through TCA-20 and 2.97, 2.86, 2.38 and 2.27 eV for TCN-0.2 through TCN-20. The increased absorption of visible light can be seen even at moderate Ce:Ti ratios, such as 5 mol%.

Photoluminescence spectra presented in Figure S5 were collected at the excitation wavelength of 365 nm. T-0 exhibits two peaks at 419 nm and 437 nm. As the Ce:Ti ratio increases, the peak at 437 nm increases compared to the peak at 419 nm. No apparent differences are observed between the TCA and TCN samples of the same Ce:Ti ratios.

The photocatalytic activity was measured for degradation of isopropanol into acetone and expressed as acetone formation rate in $ppm \cdot h^{-1}$. For this test, we included also previously-reported mesoporous TiO_2-CeO_2 composites[36] synthesized via EISA method. The composites were synthesized by introducing separately-synthesized CeO_2 into: (i) a reaction mixture during TiO_2 synthesis (TCO samples) and (ii) a physical mixture with synthesized TiO_2 (PM samples). These materials had the same Ce:Ti ratios as TCA and TCN materials: 0.2–20 mol%. TCO

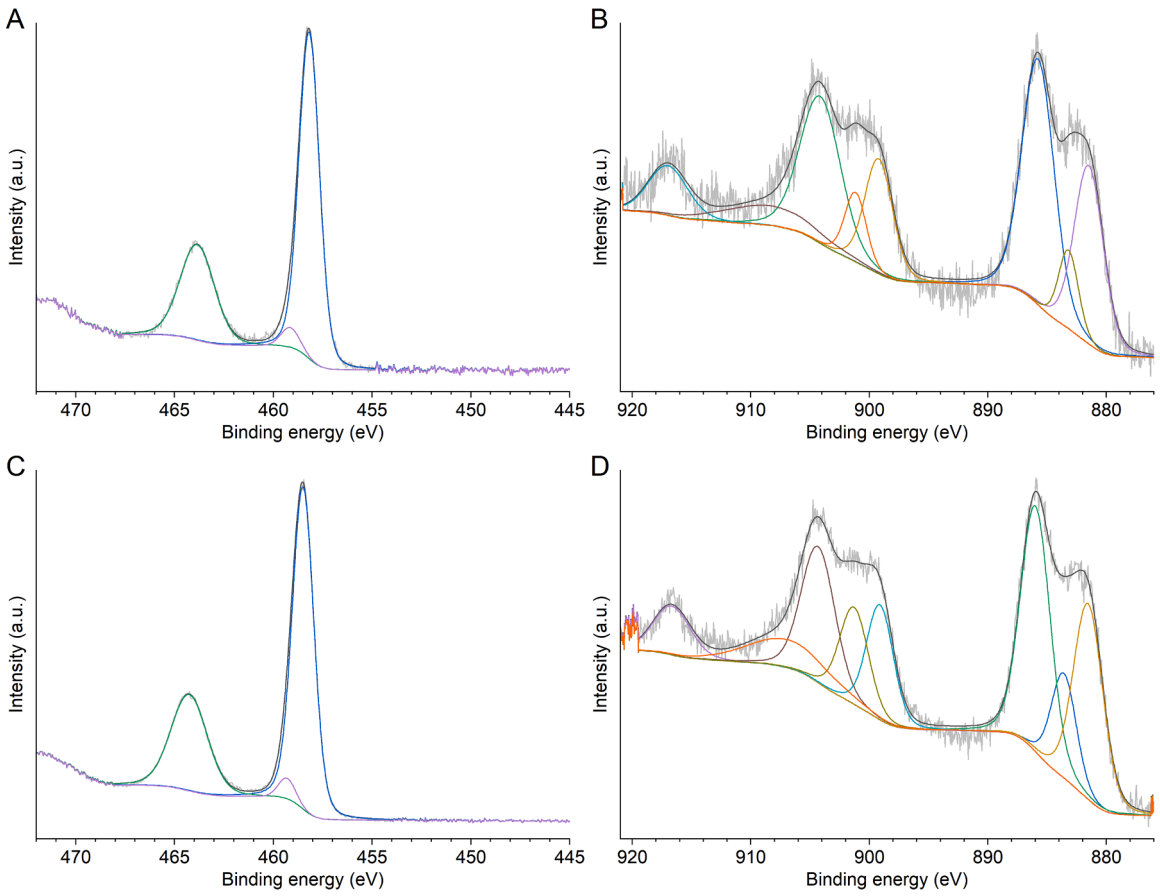

Fig. 3. XPS spectra of TCA-20 (A: Ti 2p, B: Ce 3d) and TCN-20 (C: Ti 2p, D: Ce 3d).

and PM composites had type IV isotherms with a comparable pore size distribution, lower BET specific surface area compared to TCA and TCN (up to 150 $m^2 \cdot g^{-1}$) and comparable pore volume. The crystallinity of TCO and PM did not decrease with increasing Ce:Ti ratio and anatase, the major phase, had crystallite size in the range of 8–9 nm for all Ce:Ti ratios. Crystalline CeO_2 (cerianite) was detected at higher Ce:Ti ratios. Contrary to TCA and TCN, the absorption of visible light did not increase with increasing Ce:Ti ratio in TCO and PM. To evaluate the stability of the photocatalysts, we measured each sample consecutively three times. TCA and TCN materials exhibited comparable activity for the same amount of cerium species used in the synthesis as presented in Fig. 5. Activity significantly diminished with higher Ce:Ti ratios, which can be attributed to significant decrease of crystallinity from 5 to 20 mol% materials. TCO samples had higher activity, roughly comparable to TiO_2 alone (T-0 and PM-0 (pure TiO_2 prepared according to the procedure for PM samples but without the cerium compounds)) and P25. Higher crystallinity of TCO compared to TCA and TCN could be responsible for higher activity at the same Ce:Ti ratios. We can observe that very small amounts of added CeO_2 (particularly, 0.2 mol%) produced material with at least 10 % higher activity compared to pure TiO_2. Pure CeO_2 had negligible activity (data not shown). An important distinction is, however, higher stability – smaller diminishing of activity in subsequent measurements compared to P25. TiO_2 alone (calcined once or twice) retains approx. 100 % of its initial activity, while TCO samples retain more than 90 %. P25, on the other hand, showed a higher decrease – to around 80 % of initial activity. The PM samples exhibited by far the highest activity of all sample groups, however, their activity diminished considerably after the first measurement and partially also after the second measurement (to approx. 75–85 % and 70–82 % of the initial value for the second and the third measurements, respectively). Both pure TiO_2 (T-0 and PM-0) show negligible differences, therefore any difference between the samples cannot be attributed to the effect of different number of calcination steps on TiO_2 (one for TCA, TCN and TCO; two for PM). High photocatalytic activity of PM in the first cycle could be produced by the effect of two calcination processes on CeO_2. Decrease of activity in subsequent cycles was only observed in the presence of CeO_2, but not in the control without CeO_2 (PM-0) nor in TCO samples. This initial high activity and subsequent decrease could therefore stem from cerium ability to shift between Ce^{3+} and Ce^{4+}.

4. Conclusions

We have synthesised 8 mesoporous Ti-Ce oxides using two cerium salts and with Ce:Ti molar ratios between 0.2 and 20 mol%. The materials exhibited high specific surface area (up to 180 $m^2 \cdot g^{-1}$) and pore sizes in the 3–20 nm range. Ce:Ti ratio had a significant effect on the structural and chemical properties of the products. An increase of Ce:Ti ratio decreased crystallinity and photocatalytic performance, determined as oxidation of isopropanol into acetone, even at relatively low ratios (5 mol%), even though these materials had comparable BET specific surface area and pore volume to materials with lower Ce content. On the contrary, TiO_2-CeO_2 composites (TiO_2 synthesised in the presence of CeO_2 (TCO) and physical mixture of CeO_2 and TiO_2 (PM)) showed an improved photocatalytic activity compared to pure TiO_2. While TCO composites had lower activity, they exhibited higher stability of their activity over three consecutive cycles compared to physical mixtures and P25. Presumably, the lower crystallinity of TCA and TCN materials with a high Ce:Ti ratio is responsible for their lower photocatalytic activity. We postulate that the possible formation of Ce-O-Ti species or Ce-oxide layer on TiO_2 in TCA and TCN samples compromised crystallisation during calcination process. Such interaction between Ti and Ce species was not possible in TCO and PM composites,

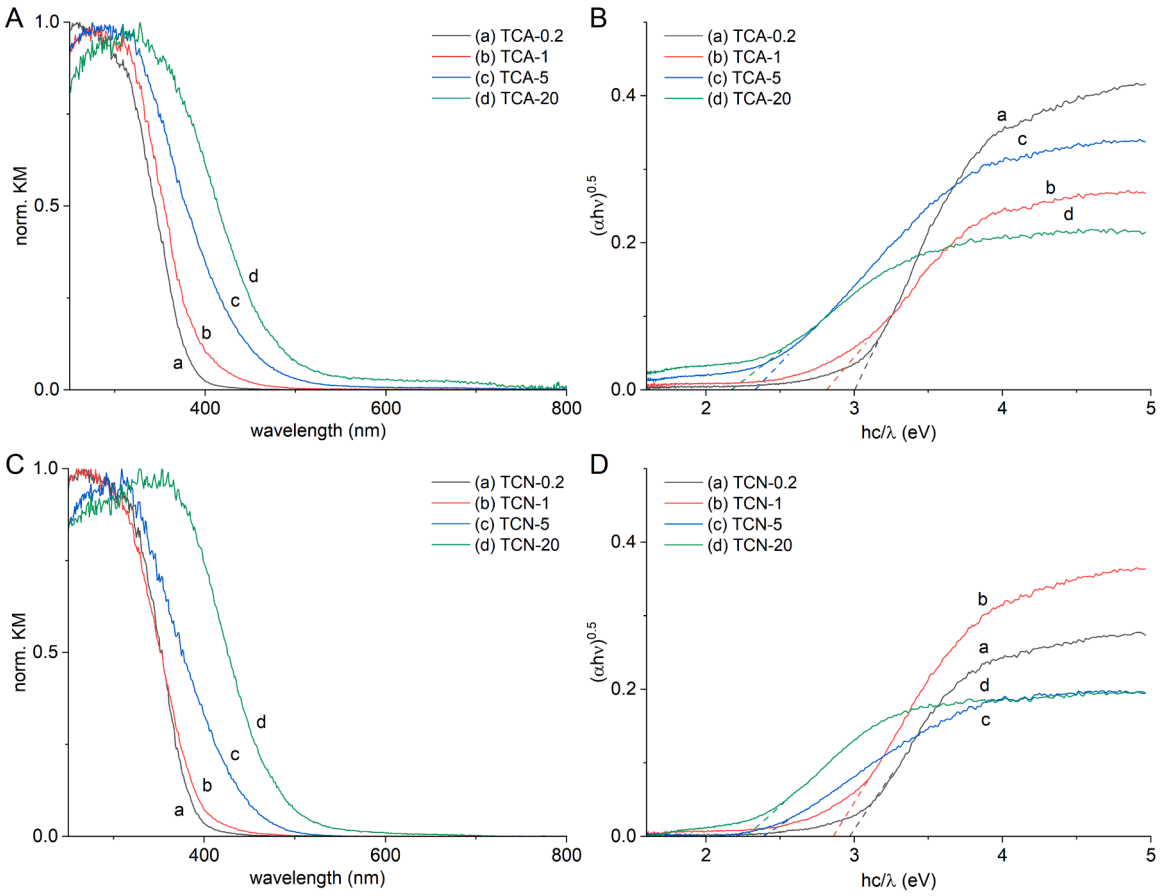

Fig. 4. Normalized Kubelka-Munk transformations of the reflectance spectra for Ti-Ce oxides for (A) TCA and (C) TCN and calculated Tauc plots for (B) TCA and (D) TCN.

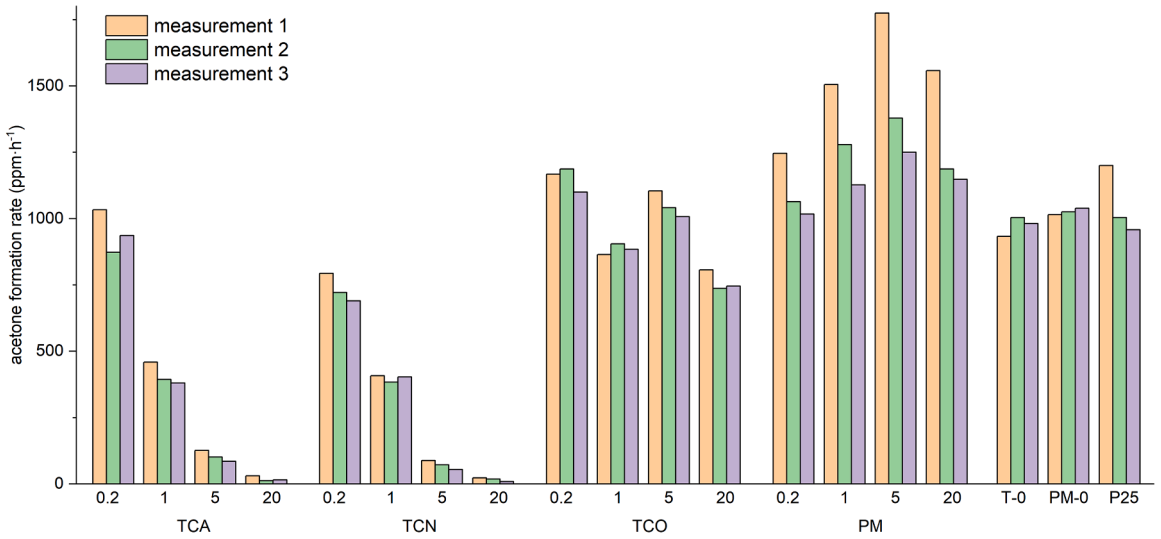

Fig. 5. Photocatalytic activity of the synthesized Ti-Ce oxides: TCA and TCN (this article), TCO and PM (synthesis and structural characterization in ref.[36]). T-0 and PM-0 are pure TiO_2, calcined once and twice, respectively. P25 is a commercial sample of photocatalytic TiO_2.

where CeO_2 was already formed before the introduction of Ti precursor and TiO_2, respectively.

CRediT authorship contribution statement

Urška Lavrenčič Štangar: Writing – review & editing, Resources, Project administration, Funding acquisition, Conceptualization. **Andrijana Sever Škapin:** Writing – review & editing, Resources, Project administration, Funding acquisition. **Tatiparthi Vikram Sagar:** Writing – review & editing, Investigation. **Mateja Knap:** Writing – original draft, Investigation. **Peter Nadrah:** Writing – original draft, Visualization, Supervision, Methodology, Investigation, Conceptualization.

Declaration of Competing Interest

The authors declare that they have no known competing financial interests or personal relationships that could have appeared to influence the work reported in this paper.

Acknowledgements

We thank Edi Kranjc for XRD analyses and dr. Gregor Marolt and Jernej Imperl for ICP-OES analyses. The authors acknowledge the financial support by the Slovenian Research and Innovation Agency (Grants no. N2-0188, J2-4441, P1-0134 and P2-0273).

Appendix A. Supporting information

Supplementary data associated with this article can be found in the online version at doi:10.1016/j.cattod.2025.115204.

Data Availability

Data will be made available on request.

References

[1] C. Xia, T. Hong Chuong Nguyen, X. Cuong Nguyen, S. Young Kim, D.L.T. Nguyen, P. Raizada, P. Singh, V.-H. Nguyen, C. Chien Nguyen, V. Chinh Hoang, Q. Van Le, Fuel 307 (2022) 121745.
[2] H.K. Paumo, S. Dalhatou, L.M. Katata-Seru, B.P. Kamdem, J.O. Tijani, V. Vishwanathan, A. Kane, I. Bahadur, J. Mol. Liq. 331 (2021) 115458.
[3] L. Yuan, M.-Y. Qi, Z.-R. Tang, Y.-J. Xu, Angew. Chem. Int Ed. 60 (2021) 21150–21172.
[4] Y. Wang, J. Zhao, T. Wang, Y. Li, X. Li, J. Yin, C. Wang, J. Catal. 337 (2016) 293–302.
[5] A.V. Emeline, A.V. Rudakova, V.K. Ryabchuk, N. Serpone, Curr. Opin. Green. Sustain. Chem. (2022) 100588.
[6] N. Rozman, P. Nadrah, R. Cornut, B. Jousselme, M. Bele, G. Dražić, M. Gaberšček, Š. Kunej, A.S. Škapin, Int. J. Hydrog. Energ. 46 (2021) 32871–32881.
[7] X. Wang, H. Xu, X. Luo, M. Li, M. Dai, Q. Chen, H. Song, Colloid Interface Sci. Commun. 44 (2021) 100476.
[8] D.P.H. Tran, M.-T. Pham, X.-T. Bui, Y.-F. Wang, S.-J. You, Sol. Energy 240 (2022) 443–466.
[9] X. Gao, Y. Jiang, Y. Zhong, Z. Luo, K. Cen, J. Hazard. Mater. 174 (2010) 734–739.
[10] L. Mahoney, R.T. Koodali, Materials 7 (2014) 2697–2746.
[11] L. Chen, B. Yao, Y. Cao, K. Fan, J. Phys. Chem. C. 111 (2007) 11849–11853.
[12] J.H. Pan, W.I. Lee, Chem. Mater. 18 (2006) 847–853.
[13] J.H. Pan, X.S. Zhao, W.I. Lee, Chem. Eng. J. 170 (2011) 363–380.
[14] K. Lan, L. Liu, J. Yu, Y. Ma, J.-Y. Zhang, Z. Lv, S. Yin, Q. Wei, D. Zhao, JACS Au 3 (2023) 1141–1150.
[15] G. Li, D. Zhang, J.C. Yu, Phys. Chem. Chem. Phys. 11 (2009) 3775–3782.
[16] M. Li, S. Zhang, L. Lv, M. Wang, W. Zhang, B. Pan, Chem. Eng. J. 229 (2013) 118–125.
[17] P. Seeharaj, N. Vittayakorn, J. Morris, P. Kim-Lohsoontorn, Nanotechnology 32 (2021) 375707.
[18] B. Palanisamy, C.M. Babu, B. Sundaravel, S. Anandan, V. Murugesan, J. Nanosci. Nanotechnol. 13 (2013) 2573–2581.
[19] X. Liu, C. Bao, Z. Zhu, H. Zheng, C. Song, Q. Xu, Int. J. Hydrog. Energy 46 (2021) 26741–26756.
[20] J. Xiao, T. Peng, R. Li, Z. Peng, C. Yan, J. Solid State Chem. 179 (2006) 1161–1170.
[21] R. Zheng, Z. Wang, C. Zhang, B. Chen, H. San, H. Yu, Compos. Part B: Eng. 222 (2021) 109037.
[22] D. Yu, Y. Liu, Z. Wu, Catal. Commun. 11 (2010) 788–791.
[23] J.C. Cano-Franco, M. Álvarez-Láinez, Mater. Sci. Semicond. Process. 90 (2019) 190–197.
[24] F. Galindo-Hernández, R. Gómez, J. Photochem. Photobiol. A: Chem. 217 (2011) 383–388.
[25] H. Shen, X.-W. Huang, I.-R. Ie, C.-S. Yuan, S.-W. Wang, ACS Omega 5 (2020) 1796–1804.
[26] F. Zheng, F. Dong, L. Zhou, J. Yu, X. Luo, X. Zhang, Z. Lv, L. Jiang, Y. Chen, M. Liu, J. Rare Earths 41 (2023) 539–549.
[27] G. Park, M. Kim, H. Lee, Ceram. Int. 48 (2022) 25656–25660.
[28] A. Ghasemi, T. Shahrabi, A.A. Oskuie, H. Hasannejad, S. Sanjabi, J. Alloy. Compd. 504 (2010) 237–242.
[29] M. Zaharescu, A. Wittmar, V. Teodorescu, C. Andronescu, M. Wittmar, M. Veith, Z. F. üR. Anorg. und Allg. Chem. 635 (2009) 1915–1924.
[30] S. Pavasupree, Y. Suzuki, S. Pivsa-Art, S. Yoshikawa, J. Solid State Chem. 178 (2005) 128–134.
[31] Y. Zhu, G. Li, S. Zhang, J. Song, C. Mao, H. Niu, B. Jin, Y. Tian, Electrochim. Acta 56 (2011) 7550–7554.
[32] C. Karunakaran, P. Navamani, P. Gomathisankar, J. Iran Chem. So.c 12 (2015) 75–80.
[33] Y. Li, W. Li, F. Liu, M. Li, X. Qi, M. Xue, Y. Wang, F. Han, J. Nanopart. Res. 22 (2020) 122.
[34] I.A. Mejia-Estrella, A. Pérez Larios, B. Sulbarán-Rangel, C.A. Guzmán González, Materials 15 (2022) 6784.
[35] Z. Zhu, D. He, Fuel 87 (2008) 2229–2235.
[36] Mateja Knap, Ur.ška Lavrenčič Štangar, Andrijana Sever Škapin, Miroslava Filip Edelmannová, Kamila Kočí, Peter Nadrah, *submitted*, DOI 10.5281/zenodo.13740586.
[37] G. Xiao, X. Huang, X. Liao, B. Shi, J. Phys. Chem. C. 117 (2013) 9739–9746.
[38] M. Myilsamy, V. Murugesan, M. Mahalakshmi, Appl. Catal. A: Gen. 492 (2015) 212–222.
[39] Q. Tang, J. He, L. Jiang, Y. Yang, J. Wang, Colloids Surf. A: Physicochem. Eng. Asp. 699 (2024) 134646.
[40] T.V. Sagar, N. Sreelatha, G. Hanmant, M. Surendar, N. Lingaiah, K.S.R. Rao, C.V. V. Satyanarayana, I. a K. Reddy, P.S.S. Prasad, RSC Adv. 4 (2014) 50226–50232.
[41] T.V. Sagar, N. Sreelatha, G. Hanmant, K. Upendar, N. Lingaiah, K.S.R. Rao, C.V. V. Satyanarayana, I. a K. Reddy, P.S.S. Prasad, Indian J. Chem. Sect. A (2014).
[42] T.V. Sagar, P. Kumar, M.F. Edelmannová, R. Ricka, M. Reli, K. Kočí, P. Nadrah, S. Emin, A.S. Škapin, U.L. Štangar, J. Environ. Chem. Eng. 12 (2024) 112072.
[43] S. Watanabe, X. Ma, C. Song, J. Phys. Chem. C. 113 (2009) 14249–14257.
[44] N.Y. Kim, H.K. Lee, J.T. Moon, J.B. Joo, Catalysts 9 (2019) 491.
[45] Z. Zhang, P.A. Maggard, J. Photochem. Photobiol. A: Chem. 186 (2007) 8–13.
[46] Z. Liu, L. Xing, H. Ma, L. Cheng, J. Liu, J. Yang, Q. Zhang, Environ. Prog. Sustain. Energy 36 (2017) 494–504.